Echo State Property of Neuronal Cell Cultures

Tomoyuki Kubota[1(✉)], Kohei Nakajima[2], and Hirokazu Takahashi[2]

[1] Department of Advanced Interdisciplinary Studies, Graduate School of Engineering, The University of Tokyo, 4-6-1 Komaba, Meguro-ku, Tokyo 153-8904, Japan
t.kubota@ne.t.u-tokyo.ac.jp

[2] Graduate School of Information Science and Technology, The University of Tokyo, 7-3-1 Hongo, Bunkyo-ku, Tokyo 113-8654, Japan

Abstract. Physical reservoir computing (PRC) utilizes the nonlinear dynamics of physical systems, which is called a reservoir, as a computational resource. The prerequisite for physical dynamics to be a successful reservoir is to have the echo state property (ESP), asymptotic properties of transient trajectory to driving signals, with some memory held in the system. In this study, the prerequisites in dissociate cultures of cortical neuronal cells are estimated. With a state-of-the-art measuring system of high-dense CMOS array, our experiments demonstrated that each neuron exhibited reproducible spike trains in response to identical driving stimulus. Additionally, the memory function was estimated, which found that input information in the dynamics of neuronal activities in the culture up to at least 20 ms was retrieved. These results supported the notion that the cultures had ESP and could thereby serve as PRC.

Keywords: Neuronal cell culture · Physical reservoir computing · Echo state property · Memory capacity

1 Introduction

Neural activity does not have permanently stable or periodic states and shows transient responses, with states moving constantly from one to the next [5,30]. For example, when a locust perceives an odor, neurons in the antenna lobe transit from low to high frequency states. Subsequently, states are maintained for a while, after which they return to the original state. The trajectory of the state transition is reproducible, but it changes depending on the stimulus duration [7].

Such a reproducible response is described by common-signal-induced synchronization or generalized synchronization [18]. When a drive subsystem and a response subsystem are represented by the states $\boldsymbol{x}$ and $\boldsymbol{y}$, respectively, the response subsystem given the time series input $\boldsymbol{h}(\boldsymbol{x})$ from the drive subsystem, converges to the state where $\boldsymbol{y}$ is represented by $\boldsymbol{y} = \boldsymbol{\Phi}(\boldsymbol{x})$, draws a repeatable trajectory for the same time series input [18]. Jaeger called such a trajectory a

I. V. Tetko et al. (Eds.): ICANN 2019, LNCS 11731, pp. 137–148, 2019.
https://doi.org/10.1007/978-3-030-30493-5_13

transient attractor [11] and the property of converging to this trajectory an echo state property (ESP) [13,20]. Reservoir computing (RC) [14,19,31] generates reproducible responses by generalized synchronization between the drive and response subsystem such as a recurrent neural network (RNN) composed of sigmoid or spiking neurons, and emulates desired outputs by linear regression with the reproducible responses. RC can not only be applied in engineering, such as in machine learning, but can also be used to estimate computational capabilities of a dynamical system by analyzing equations executed in the response subsystem, i.e., in the reservoir. For example, by letting a reservoir learn past inputs, we can examine how accurately and how long the inputs would be retained in the reservoir [12].

Furthermore, physical reservoir computing (PRC), which uses a physical system as a reservoir, has been reported in recent years. The framework of RC at least requires generalized synchronization between the drive subsystem and response subsystem to construct a successful reservoir, and to date, various dynamical systems have been utilized as reservoirs, and their computational capabilities have been evaluated by many researchers, as follows: Fernando et al. showed that ripples changing temporally in a bucket have linear separability [8]. Recently, the computational capabilities of delay-based dynamical systems were analyzed by applying time-multiplexing to electronic and laser systems subject to delay feedback and thereby constructing a pseudo network [1,4]. Furthermore, Nakajima et al. applied forces to a device mimicking an octopus arm and investigated its computational capabilities from a dynamical system's point of view [21–26].

As discussed previously, PRC has been applied to various dynamical systems to evaluate their computational capabilities; however, in real neural circuits, synaptic plasticity works according to the long-term input history, and the network structure between neurons is constantly updated and the response of the circuits would alter accordingly [9,16]. Furthermore, computational capabilities of RNNs such as timing capacity, which is the maximum delay after a pulse input that the network produces, have been analyzed [17], whereas PRC with cultures has not been achieved. On the other hand, Dranias et al. evaluated short-term memory combining transient dynamics of cell cultures and support vector machine (SVM), and showed that the cultures discriminated input applied 1 s or more before [6]. However, as SVM was adopted for the readout, responses retrieved from the culture were nonlinearly transformed and one can not distinguish nonlinearity of the culture's responses from of SVM. Therefore, the characteristics of neuronal cultures as reservoirs have not been fully revealed.

In this paper, we constructed a reservoir using a cell culture from rat cortices and stimulated it two times with an identical electrical stimulation trace to investigate whether the reservoir met the prerequisite for RC, i.e., whether it has an ESP. Additionally, we examined their expressive capability of information by measuring memory functions.

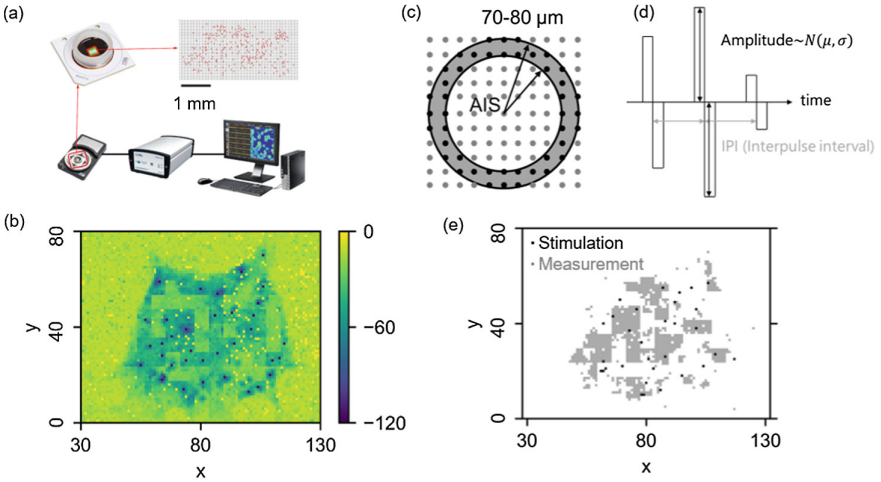

Fig. 1. Composing a reservoir with a rat cortical cell culture. (a) Micro-electrode array (MEA) system. (b) The mean extracellular action potential (EAP) amplitudes of spontaneous activity plotted on the electrode array at 46 days in vitro (DIV). Black points represent electrodes in the vicinity of axon initial segments (AIS). (c) The axons were located by sequentially stimulating electrodes that were included in the area having a radius 70–80 µm from the AIS. The black points are the stimulated electrodes. (d) The waveform of bipolar pulse stimulation. The amplitude follows a normal distribution, and the interpulse interval (IPI) is 10, 20, or 30 ms. (e) The selected electrodes used for measurement (gray) and stimulation (black).

2 Materials and Methods

2.1 Cell Culture

All experiments were approved by the ethical committee of the University of Tokyo and followed "Guiding Principles for the Care and Use of Animals in the Field of Physiological Science" by the Physiological Society of Japan.

Techniques for cell culture have been developed to maintain the culture and conduct experiments for a long time [10,28]. Embryonic rat cortices were dissected from E18 rat and used for cortical cell cultures. The cortices were dissociated in 2 mL of 0.25% trypsin-ethylenediaminetetraacetic acid (Trypsin-EDTA, Life Technologies), from which cells were isolated by trituration, and 38,000 cells were seeded on each MEA (MaxWell Biosystems; Fig. 1(a)). For cell adhesion, 5 mL of 0.05% Polyethileneimine (PEI; Sigma-Aldrich) and 5 µL of 0.02 mg/mL Laminin (Sigma-Aldrich) were used before plating the cells. After 24 h from plating the cells, the plating media [3] were changed to the growth media [28]. The plating media were composed of Neurobasal 850 µL (Life Technologies), 10% horse serum (HyClone), 0.5 mM GlutaMAX (Life Technologies), and 2% B27 (Life Technologies). The growth media were composed of DMEM 850 µL (Life Technologies), 10% horse serum (HyClone), 0.5 mM GlutaMAX (Life Tech-

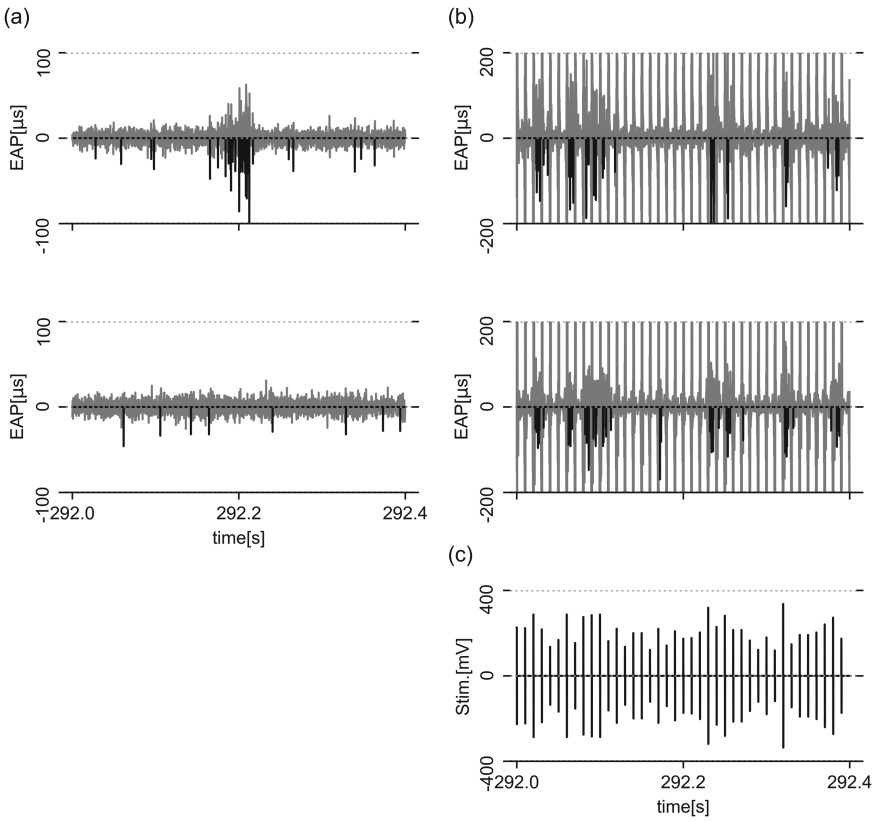

Fig. 2. Detected extracellular action potentials. The position of the measurement electrode (x, y) is (77, 35). In (a) and (b), the gray and black lines represent filtered signals and signals detected as spikes, respectively. (a) Extracellular action potentials of spontaneous activity measured before (upper) and after (lower) the stimulation. (b) Extracellular action potentials evoked by two-trial identical stimulations. Filtered signals saturated when electrical stimulation was conducted. (c) The stimulation signal trace. The mean and standard deviation of stimulation amplitude were 200 mV and 50 mV, respectively. The interpulse interval was 10 μs.

nologies), and 1 mM sodium pyruvate (Life Technologies). All experiments were conducted in an incubator at 37 °C and 5% CO_2. The MEAs were sealed with a lid to prevent water evaporation and invasion of bacteria and fungus.

2.2 Electrode Selection

We calculated the average spike amplitudes during a spontaneous activity at all electrodes, and selected electrodes on which the axon places as stimulation electrodes. The MEA had 26,400 electrodes, which place 17.5 μm apart and are arranged in a 120 × 220 grid. An extracellular action potential (EAP) has

a larger negative amplitude in the vicinity of an axon initial segment (AIS) than around other segments [2], and the EAP amplitude of spontaneous activity at each electrode were obtained to search for electrodes near neurons among 26,400 electrodes. We first obtained 20-s voltage traces at 26,400 electrodes, from which negative EAPs $\boldsymbol{x}_n$ were detected. From these $\boldsymbol{x}_n$, the average of the EAP amplitudes for each electrode were calculated to create a 120×220 map. We smoothed the electrode map using the Gaussian filter, searched local minima on the map, and regarded them as electrodes near AISs. Furthermore, to search for the axon of the AIS, all electrodes in an area with a radius of 70–80 μm from the AIS electrodes were stimulated one at a time. As shown in Fig. 1(c), each electrode was stimulated by 20 bipolar pulses with 50-ms interpulse interval (IPI) and 300-mV amplitude. Spike detection was applied to the voltage traces to obtain band-pass filtered signals. The signal traces for 20 trials were averaged and electrodes whose mean amplitude could be less than $-200\,\mu\mathrm{V}$ were selected as the stimulation electrodes.

The AIS electrodes and electrodes with a high firing rate were chosen as the measurement electrodes. The MEA could simultaneously utilize up to 1,024 of 26,400 electrodes. The remaining electrodes, except the stimulation and AIS electrodes, were connected to the electrodes with a higher firing rate. To measure the number of spikes at each electrode, voltage traces in spontaneous activity were measured for 20 s each.

2.3 Spike Detection

The 6^{th} Butterworth bandpass filter and zero-phase IIR filter were applied to the voltage traces to extract 300–3000 Hz components. For stimulating electrodes, artifacts caused by stimulation were removed by eliminating traces ±2 ms from the stimulation times. The extracted signals were divided into positive components $\boldsymbol{x}_p$ and negative components $\boldsymbol{x}_n$, and their standard deviations were calculated as follows [29]:

$$\sigma = \mathrm{median}\left\{\frac{|\boldsymbol{x}|}{0.6745}\right\}. \tag{1}$$

If the amplitude of extracted signal exceeded 4σ ($\boldsymbol{x}_p > 4\sigma_p, |\boldsymbol{x}_n| > 4\sigma_n$), the value of spike train was set to one; otherwise, it was set to zero. There is a 1–2 ms period called absolute refractory period, in which spikes do not occur even when the neuron is stimulated. As the measurement frequency was 20 kHz, the above spike train was separated by a 1-ms time bin, and if one or more spikes appeared in one bin, the modified spike train was set to one; otherwise it was set to zero.

2.4 Electrical Stimulation

When investigating ESP and memory capacity, we gave bipolar pulse stimuli (Fig. 1(c)) of the amplitude that followed the normal distribution $\mathcal{N}(\mu, \sigma^2)$ with mean μ and standard deviation σ, and of the IPI of $T = 10$, 20, and 30 ms.

2.5 Spike Metric

The distance between two spike trains were evaluated with Victor's spike metric [32]. Two vectors $\boldsymbol{a} \in \mathbf{N}^{n_a}$ and $\boldsymbol{b} \in \mathbf{N}^{n_b}$ $(n_a \leq n_b)$ hold spike times in the first and second trials, respectively, and the total cost to convert $\boldsymbol{a}$ to $\boldsymbol{b}$ is calculated. Although there are many conversion paths, the one with the minimum cost among them is the distance $G(\boldsymbol{a}, \boldsymbol{b})$. To convert the vector, there are three operations: adding, deleting, and moving spikes, whose costs are one, one, and $q\,\Delta t$, respectively. Note that Δt is the absolute difference between the times before and after moving the spike, and q is a weight parameter and was set to 10 ms. As the distance $G(\boldsymbol{a}, \boldsymbol{b})$ depends on n_a, n_b, the normalized distance $d(\boldsymbol{a}, \boldsymbol{b})$ was obtained as follows:

$$d(\boldsymbol{a}, \boldsymbol{b}) = \frac{G(\boldsymbol{a}, \boldsymbol{b}) - \Delta n}{n_a}. \tag{2}$$

When Victor's metric converts $\boldsymbol{a}$ to $\boldsymbol{b}$, spikes are added $\Delta n (= n_b - n_a)$ times. Since the spike addition cost is one, there will always be a cost Δn. The remaining n_a spikes are transformed by moving, or adding and deleting, and $d(\boldsymbol{a}, \boldsymbol{b})$ represent the cost averaged over n_a operations.

2.6 Composing a Reservoir

The interpulse interval was T (= 10, 20, 30 ms), whereas the spike detection interval was 1 ms. Since the two intervals must be the same to compose a reservoir, the spike count in a T-width time bin was used as a state of node.

When a dynamical system has computational capabilities, the system converges to the same trajectory without depending on the initial values [13,20]. To wash out the initial transient, the time series data after converging was divided into training data $(i = 1, \cdots, N)$ and test data $(i = N+1, \cdots, 2N)$.

Ridge regression was adopted for training readout weights. The readout weights $\boldsymbol{w}$ and the output $\hat{y}$ were calculated by Eqs. (3) and (4), respectively.

$$\hat{\boldsymbol{w}} = \arg\min_{\boldsymbol{w}} \left\{ \frac{1}{N} \sum_{i=1}^{N} (y_i - \boldsymbol{w} \cdot \boldsymbol{s}_i)^2 + \alpha ||\boldsymbol{w}||_2^2 \right\}, \tag{3}$$

$$\hat{y}_i = \hat{\boldsymbol{w}} \cdot \boldsymbol{s}_i, \tag{4}$$

where y_i was the desired output in the i-th time bin, $||\cdot||_2$ representing the Euclidean norm, and α was a hyperparameter that adjusts the degree of normalization. When one uses Ridge regression, the Akaike information criteria AIC is expressed by the following equation:

$$AIC = \frac{1}{N\hat{\sigma}^2} \left(\sum_{i=N+1}^{2N} (\hat{y}_i - y_i)^2 + 2\hat{\sigma}^2 df \right), \tag{5}$$

$$df = \sum_{i=1}^{M+1} \frac{e_i}{e_i + \alpha}, \tag{6}$$

where $\hat{\sigma}^2 = \frac{1}{N-p-1}\sum_{i=N+1}^{2N}(\hat{y}_i|_{\alpha=0} - y_i)^2$, and $e_i (i = 1, 2, \cdots, M+1)$ were the eigenvalues of the matrix $[\boldsymbol{s}_1 \cdots \boldsymbol{s}_N]^T[\boldsymbol{s}_1 \cdots \boldsymbol{s}_N]$. We obtained p pairs of $(\alpha, \boldsymbol{w})$ during training and p pairs of (α, AIC) during test, with which α was chosen such that the AIC would be minimized.

2.7 Memory Capacity

A measure for short-term memory of a reservoir is memory capacity (MC), which quantifies the past input held in the reservoir by giving the temporally uncorrelated time-series input ν_i to the reservoir and emulating the past inputs. The memory function f_k $(k = 1, 2, \cdots)$ represents the accuracy with which ν_{i-k} the input delayed by k time bin are stored in the reservoir and examining f_k provides how accurately and how long the input is held. The memory capacity C is represented by the sum of f_k:

$$f_k = \max_{\boldsymbol{w}} \frac{\left(\sum_i (\nu_{i-k} - \bar{\nu})(\hat{y}_i - \bar{\hat{y}})\right)^2}{\sum_i (\nu_i - \bar{\nu})^2 \cdot \sum_i (\hat{y}_i - \bar{\hat{y}})^2} \tag{7}$$

$$C = \sum_k f_k \tag{8}$$

3 Results and Discussions

3.1 Echo State Property

Spontaneous activities and evoked responses were alternately measured for 300 s per trial. Figure 2(a) and (b) show the filtered signals of spontaneous activity and evoked responses at 292.0–292.4 s, respectively. Figure 2(c) represents the stimulation voltage trace applied to all stimulation electrodes. While the spike frequency in spontaneous activity was low and the spike times were uniformly distributed, the spikes in evoked response densely concentrated around specific times, which corresponded with times when the amplitude was large and indicated that strong stimuli induced spikes at specific times.

Figure 3 shows the difference in the number of spikes, Δn, and the normalized spike train distance, d, with 1-s time bin. Δn converged in approximately 30 s from beginning of stimulation whereas d fluctuated a little before Δn converged; therefore, the spike trains converged in approximately 30 s, which suggests that short-term plasticity occurred in the culture. The spikes in each neuron might converge because of facilitation and depression caused by repeated spikes occurrence.

Furthermore, the spike train distances of spontaneous activities and evoked responses with 300-s time bin are shown in Fig. 4(a) and (b), respectively, where the distances were calculated for each activity and plotted on the electrode map. In addition, the averaged distances for 80 electrodes of all the measurement electrodes are shown in Fig. 4(c). The average distances of spontaneous activity were close to two, which indicated that there were many pairs whose spike time

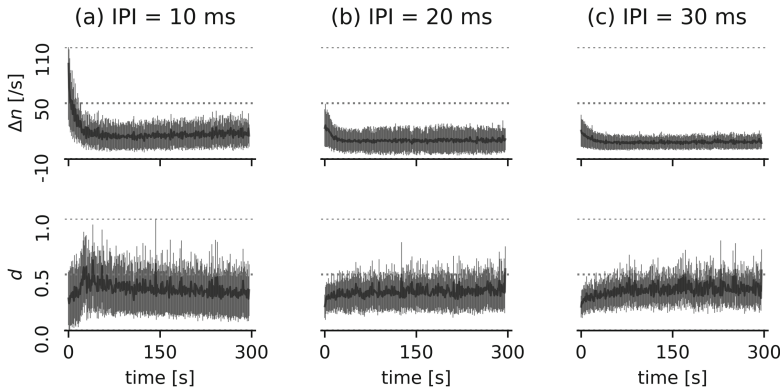

Fig. 3. The average spike train distance changes in time ($\mu = 200\,\mathrm{mV}$). The upper and lower figures show the absolute difference in the number of spikes Δn and the normalized distance d. The figures (a), (b), and (c) show the distances when the interpulse interval is 10, 20, and 30 ms, respectively. The black lines and shade are the mean distances and the standard deviation over the measurement electrodes, respectively.

differences were more than 10 ms because the cost to delete and add the spike ($\Delta t > 10\,\mathrm{ms}$) is two. However, the average distances of evoked responses were smaller than those of spontaneous activity, which suggests that the spikes with a time difference of 10 ms or less increased in evoked responses. The distances in evoked responses being smaller than those in spontaneous activity indicated that the cell culture had the ESP.

Additionally, Fig. 4(d) shows the average distances for the mean amplitude μ and IPI of the stimulus. As μ and IPI increased, the average distance decreased. Spike trains were measured in some trials when a bipolar pulse stimulus with 2.4-V amplitude was injected, and the reproducibility between spikes was examined [15], where spikes occurred in 10 ms or more after stimulation and the spike patterns matched better as the spike times were closer to the stimulation. In contrast, when stimulation was repeatedly applied to the cell culture, the spike train distance got smaller as the IPI was larger, which might imply that when multiple stimulations were given, the spike timing was well-matched to a time close to 30 ms from the stimulation.

3.2 Memory Functions

We constructed a reservoir with nodes whose state was the spike number within a time bin T (= 10, 20, and 30 ms) and calculated the memory functions. Figure 5 shows the memory functions of the cortical cell culture. ρ_k represents the correlation coefficient of ν_{i-k} with $\hat{y}_i$ that was calculated with $\boldsymbol{w}$ of the memory function f_k. ρ_k (Fig. 5(a) $k = 1, 2$, (b) $k = 1$, and (c) $k = 1$) showed weak positive correlations, which proved that the number of spikes was determined by stimulation up to 20 ms. It has been reported that spikes for 20 ms from the

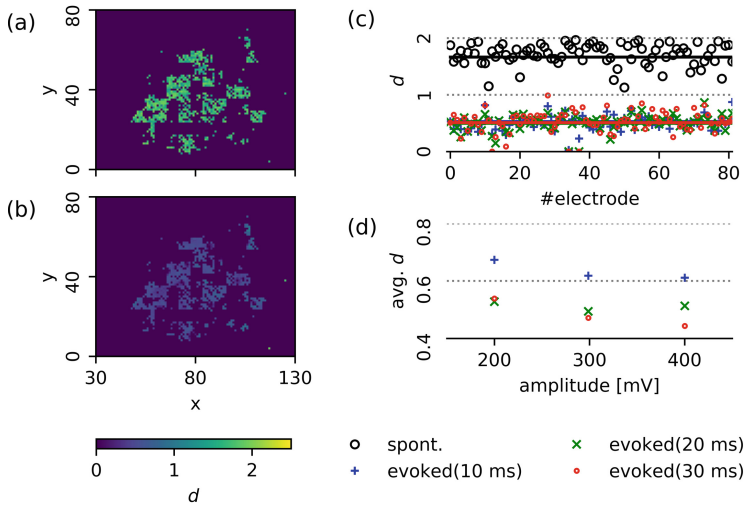

Fig. 4. Echo state property of a rat cortical cell culture. (a) Spike train distances of spontaneous activities on the electrode array. (b) Spike train distances of evoked activities on the electrode array. The interpulse interval (IPI) was 10 ms. (c) Spike train distances of each electrode. 80 of all measurement electrodes are shown here. The colored lines show the mean distances of all electrode distances. In (c) and (d), black circle, blue plus, green cross, and red circle markers stand for spontaneous activity and evoked response with 10, 20, and 30-ms IPI stimulations, respectively. In (b) and (c), mean and standard deviation of stimulation amplitude were 300 mV and 50 mV, respectively. (d) Distances averaged over all measurement electrodes except for stimulation ones. The standard deviation of stimulation amplitude was 50 mV. (Color figure online)

stimulus are caused by the stimulus. These results showed that the number of spikes was determined not only by the stimulus just before but by stimuli up to 20 ms before. A part of stimulus information up to 20 ms before might be retained by excitatory postsynaptic potentials (EPSPs) of pyramidal neurons. If a next EPSP occurs before the previous EPSP returns to the base line, the EPSP is added up. The addition of EPSP is linear when the interval is 30 ms or more, and nonlinear when it is 30 ms or less [27]. As the stimulus is stronger, the stimulated neuron fire more frequently and the postsynaptic neurons retain more nonlinear EPSPs. In other words, the number of spikes of postsynaptic neurons might have contributed to the stimulus strength information held in the reservoir.

However, the stimulation amplitudes older than 20 ms were not retained. Dranias et al. optically stimulated cell cultures where neurons were transfected with ChannelRhodopsin-2, and showed that SVM with time series data of firing rate could distinguish optical stimulations applied 1 s or more before [6]. In our study, since the stimulation interval was 10–30 ms, further studies are needed to examine what occurs in the culture when this interval is longer.

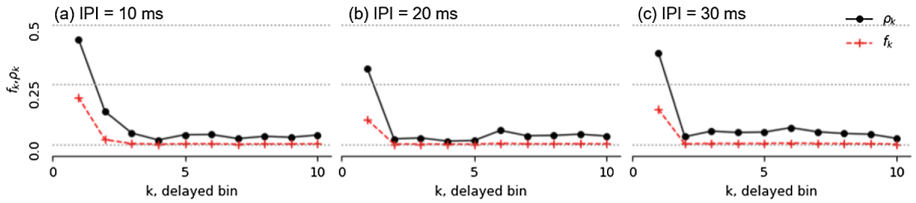

Fig. 5. Memory function of a rat cortical cell culture ($\mu = 400\,\mathrm{mV}$). The red plus markers and the black circle markers represent f_k, the memory function of k, and the correlation coefficient ρ_k, respectively. The figures (a), (b), and (c) show memory functions when interpulse interval is 10, 20, and 30 ms, respectively. (Color figure online)

4 Conclusions

In this paper, we constructed reservoirs using cell cultures from rat cortices and stimulated them two times with an identical electrical stimulation trace to measure the distance between two spike trains. Additionally, we examined their expression of information by measuring memory functions. The results were as follows:

- When the axons of spontaneously active neurons were stimulated, the spike train distances of evoked activity averaged at all electrodes were smaller than the distance of spontaneous activity.
- As the amplitude and IPI of stimulation increased, the spike train distances decreased.
- When the electrical stimulation whose amplitude followed the normal distribution was applied and the reservoir was constructed with the nodes represented by the firing rate, the memory function became relatively high at bins delayed by one and two.

Acknowledgments. This paper is based on results obtained from a project (Exploration of Neuromorphic Dynamics towards Future Symbiotic Society) commissioned by NEDO, KAKENHI grant (17K20090), AMED (JP18dm0307009) and Asahi Glass Foundation. We thank Hitachi UTokyo Laboratory, Hitachi, Ltd. for fruitful discussions. K. N. was supported by JST PRESTO Grant Number JPMJPR15E7, Japan and KAKENHI No. JP18H05472, No. 16KT0019, and No. JP15K16076.

References

1. Appeltant, L., et al.: Information processing using a single dynamical node as complex system. Nat. Commun. **2**, 468 (2011). https://doi.org/10.1038/ncomms1476
2. Bakkum, D.J., et al.: The axon initial segment is the dominant contributor to the neuron's extracellular electrical potential landscape. Adv. Biosyst. **3**(2), 1800308 (2019). https://doi.org/10.1002/adbi.201800308

3. Brewer, G.J., Torricelli, J., Evege, E., Price, P.: Optimized survival of hippocampal neurons in B27-supplemented neurobasal^{TM}, a newserum-free medium combination. J. Neurosci. Res. **35**(5), 567–576 (1993). https://doi.org/10.1002/jnr.490350513
4. Brunner, D., Soriano, M.C., Mirasso, C.R., Fischer, I.: Parallel photonic information processing at gigabyte per second data rates using transient states. Nat. Commun. **4**, 1364 (2013). https://doi.org/10.1038/ncomms2368
5. Buonomano, D.V., Maass, W.: State-dependent computations: spatiotemporal processing in cortical networks. Nat. Rev. Neurosci. **10**(2), 113 (2009). https://doi.org/10.1038/nrn2558
6. Dranias, M.R., Ju, H., Rajaram, E., VanDongen, A.M.: Short-term memory in networks of dissociated cortical neurons. J. Neurosci. **33**(5), 1940–1953 (2013). https://doi.org/10.1523/JNEUROSCI.2718-12.2013
7. Durstewitz, D., Deco, G.: Computational significance of transient dynamics in cortical networks. Eur. J. Neurosci. **27**(1), 217–227 (2008). https://doi.org/10.1111/j.1460-9568.2007.05976.x
8. Fernando, C., Sojakka, S.: Pattern recognition in a bucket. In: Banzhaf, W., Ziegler, J., Christaller, T., Dittrich, P., Kim, J.T. (eds.) ECAL 2003. LNCS, vol. 2801, pp. 588–597. Springer, Heidelberg (2003). https://doi.org/10.1007/978-3-540-39432-7_63
9. Goel, A., Buonomano, D.V.: Timing as an intrinsic property of neural networks: evidence from in vivo and in vitro experiments. Philos. Trans. R. Soc. B: Biol. Sci. **369**(1637), 20120460 (2014). https://doi.org/10.1098/rstb.2012.0460
10. Hales, C.M., Rolston, J.D., Potter, S.M.: How to culture, record and stimulate neuronal networks on micro-electrode arrays (meas). JoVE (J. Vis. Exp.) (39), e2056 (2010). https://doi.org/10.3791/2056
11. Jaeger, H.: Identification of behaviors in an agent's phase space. Citeseer (1995)
12. Jaeger, H.: Short term memory in echo state networks, vol. 5. GMD-Forschungszentrum Informationstechnik (2001)
13. Jaeger, H.: Tutorial on training recurrent neural networks, covering BPPT, RTRL, EKF and the "echo state network" approach, vol. 5. GMD-Forschungszentrum Informationstechnik Bonn (2002)
14. Jaeger, H., Haas, H.: Harnessing nonlinearity: predicting chaotic systems and saving energy in wireless communication. Science **304**(5667), 78–80 (2004). https://doi.org/10.1126/science.1091277
15. Jimbo, Y., Kawana, A., Parodi, P., Torre, V.: The dynamics of a neuronal culture of dissociated cortical neurons of neonatal rats. Biol. Cybern. **83**(1), 1–20 (2000). https://doi.org/10.1007/PL00007970
16. Johnson, H.A., Goel, A., Buonomano, D.V.: Neural dynamics of in vitro cortical networks reflects experienced temporal patterns. Nat. Neurosci. **13**(8), 917 (2010). https://doi.org/10.1038/nn.2579
17. Laje, R., Buonomano, D.V.: Robust timing and motor patterns by taming chaos in recurrent neural networks. Nat. Neurosci. **16**(7), 925 (2013). https://doi.org/10.1038/nn.3405
18. Lu, Z., Hunt, B.R., Ott, E.: Attractor reconstruction by machine learning. Chaos: Interdisc. J. Nonlinear Sci. **28**(6), 061104 (2018). https://doi.org/10.1063/1.5039508
19. Maass, W., Natschläger, T., Markram, H.: Real-time computing without stable states: a new framework for neural computation based on perturbations. Neural Comput. **14**(11), 2531–2560 (2002). https://doi.org/10.1162/089976602760407955

20. Manjunath, G., Jaeger, H.: Echo state property linked to an input: exploring a fundamental characteristic of recurrent neural networks. Neural Comput. **25**(3), 671–696 (2013). https://doi.org/10.1162/NECO_a_00411
21. Nakajima, K.: Muscular-hydrostat computers: physical reservoir computing for octopus-inspired soft robots. In: Shigeno, S., Murakami, Y., Nomura, T. (eds.) Brain Evolution by Design. DCA, pp. 403–414. Springer, Tokyo (2017). https://doi.org/10.1007/978-4-431-56469-0_18
22. Nakajima, K., Hauser, H., Kang, R., Guglielmino, E., Caldwell, D.G., Pfeifer, R.: Computing with a muscular-hydrostat system. In: 2013 IEEE International Conference on Robotics and Automation, pp. 1504–1511. IEEE (2013). https://doi.org/10.1109/ICRA.2013.6630770
23. Nakajima, K., Hauser, H., Kang, R., Guglielmino, E., Caldwell, D.G., Pfeifer, R.: A soft body as a reservoir: case studies in a dynamic model of octopus-inspired soft robotic arm. Front. Comput. Neurosci. **7**, 91 (2013). https://doi.org/10.3389/fncom.2013.00091
24. Nakajima, K., Hauser, H., Li, T., Pfeifer, R.: Information processing via physical soft body. Sci. Rep. **5**, 10487 (2015). https://doi.org/10.1038/srep10487
25. Nakajima, K., Hauser, H., Li, T., Pfeifer, R.: Exploiting the dynamics of soft materials for machine learning. Soft Robot. **5**(3), 339–347 (2018). https://doi.org/10.1089/soro.2017.0075
26. Nakajima, K., Li, T., Hauser, H., Pfeifer, R.: Exploiting short-term memory in soft body dynamics as a computational resource. J. R. Soc. Interface **11**(100), 20140437 (2014). https://doi.org/10.1098/rsif.2014.0437
27. Nettleton, J.S., Spain, W.J.: Linear to supralinear summation of AMPA-mediated EPSPs in neocortical pyramidal neurons. J. Neurophysiol. **83**(6), 3310–3322 (2000)
28. Potter, S.M., DeMarse, T.B.: A new approach to neural cell culture for long-term studies. J. Neurosci. Methods **110**(1–2), 17–24 (2001). https://doi.org/10.1016/S0165-0270(01)00412-5
29. Quiroga, R.Q., Nadasdy, Z., Ben-Shaul, Y.: Unsupervised spike detection and sorting with wavelets and superparamagnetic clustering. Neural Comput. **16**(8), 1661–1687 (2004). https://doi.org/10.1162/089976604774201631
30. Rabinovich, M., Huerta, R., Laurent, G.: Transient dynamics for neural processing. Science **321**(5885), 48–50 (2008). https://doi.org/10.1126/science.1155564
31. Verstraeten, D., Schrauwen, B., d'Haene, M., Stroobandt, D.: An experimental unification of reservoir computing methods. Neural Netw. **20**(3), 391–403 (2007). https://doi.org/10.1016/j.neunet.2007.04.003
32. Victor, J.D., Purpura, K.P.: Nature and precision of temporal coding in visual cortex: a metric-space analysis. J. Neurophysiol. **76**(2), 1310–1326 (1996). https://doi.org/10.1152/jn.1996.76.2.1310